# A new method for the semiquantitative determination of major rock-forming minerals with thermal infrared multispectral data: Application to THEMIS infrared data

Jun Huang,[1,2] Christopher S. Edwards,[3] Steven W. Ruff,[2] Philip R. Christensen,[2] and Long Xiao [1]

Received 9 July 2013; revised 5 September 2013; accepted 16 September 2013; published 10 October 2013.

[1] We have developed a new method (least residual iterative spectral mixture analysis (LRISMA)) to semiquantitatively determine major rock-forming minerals (feldspar, pyroxene, olivine, high-silica phases, and quartz) with multispectral thermal infrared data. Sublibraries of minerals are generated from a master library of minerals based on prior knowledge to produce a suite of realistic mineral end-member combinations to fit the target spectra. Mineral abundances that correspond to the least root-mean-square errors (best fit) generally agree best with previous petrographic studies of laboratory-measured rock samples and thermal infrared hyperspectral analysis of materials on the surface of Mars, given the greatly reduced spectral range and resolution of Thermal Emission Imaging System (THEMIS) spectra. The accuracy and reproducibility of LRISMA is ~4–16% and ~5–20%, respectively, while the accuracy of petrographic and previous hyperspectral studies is ~5–15%. LRISMA can be applied to semiquantitatively refine the bulk surface mineralogy of small-scale (~1 $km^2$) geologic features with high-quality THEMIS spectral data (high surface temperature: >260 K, low atmospheric opacity: total ice < 0.04 and total dust < 0.15) with the ultimate goal of better understanding regional geologic processes.

**Citation:** Huang, J., C. S. Edwards, S. W. Ruff, P. R. Christensen, and L. Xiao (2013), A new method for the semiquantitative determination of major rock-forming minerals with thermal infrared multispectral data: Application to THEMIS infrared data, *J. Geophys. Res. Planets*, *118*, 2146–2152, doi:10.1002/jgre.20160.

## 1. Introduction

[2] Infrared instruments have been used to study the compositional and thermophysical properties of Mars' surface in detail over the past few decades [e.g., *Bell*, 2008, and references therein]. Data from the Thermal Emission Spectrometer (TES) onboard Mars Global Surveyor were used to create quantitative Martian global maps of albedo, mineral abundance, and thermal inertia [e.g., *Bandfield*, 2002; *Christensen et al*., 2001; *Mellon et al*., 2000]. More recent instruments, both thermal infrared (TIR: Thermal Emission Imaging System (THEMIS)) [*Christensen et al*., 2004] and visible/near infrared (VNIR: Observatoire pour la Minéralogie, l'Eau, les Glaces et l'Activité (OMEGA)) [*Bibring et al*., 2006], and Compact Reconnaissance Imaging Spectrometer for Mars (CRISM) [*Murchie et al*., 2007] have greatly improved our understanding about the compositional, thermophysical, and paleoenvironmental characteristics of the Martian surface.

[3] It has been shown that linear least squares modeling of laboratory TIR spectra can be used to quantitatively assess the mineralogy of crystalline igneous rocks with accuracies of 5–15% [*Feely and Christensen*, 1999; *Ramsey and Christensen*, 1998]. This approach has been applied to a variety of global mineralogical studies of Mars using TES data [e.g., *Christensen et al*., 2000b; *Bandfield*, 2002; *Hamilton et al*., 2003; *Rogers and Christensen*, 2007; *Koeppen and Hamilton*, 2008]. More regional studies have combined lower spatial resolution (~3 × 6 $km^2$), higher spectral resolution (10 $cm^{-1}$ sampling) TES data to quantitatively determine the composition of representative locations and higher spatial resolution (100 m/pixel), lower spectral resolution (eight surface-sensitive bands) THEMIS data to map the distribution of the representative locations [*Bandfield et al*., 2004a; *Glotch and Christensen*, 2005; *Hamilton and Christensen*, 2005; *Rogers et al*., 2005; *Edwards et al*., 2008; *Rogers et al*., 2009; *Tornabene et al*., 2008; *Rogers and Fergason*, 2011].

[4] When the geologic features are smaller than the TES footprint on the surface of Mars, it is difficult to definitively determine the mineral abundance of these features (<3 × 6 $km^2$) from TES data. No previous work has been done to unmix atmospherically corrected THEMIS spectra with an individual mineral end-member library; rather, the standard approach is to use general basaltic and dust

[1]Planetary Science Institute, China University of Geosciences, Wuhan, Hubei, China.
[2]Mars Space Flight Facility, Arizona State University, Tempe, Arizona, USA.
[3]Division of Geological and Planetary Sciences, California Institute of Technology, Pasadena, California, USA.

Corresponding author: J. Huang, Planetary Science Institute, China University of Geosciences, Wuhan, Hubei 430074, China. (jhuang.cug@gmail.com)


2169-9097/13/10.1002/jgre.20160

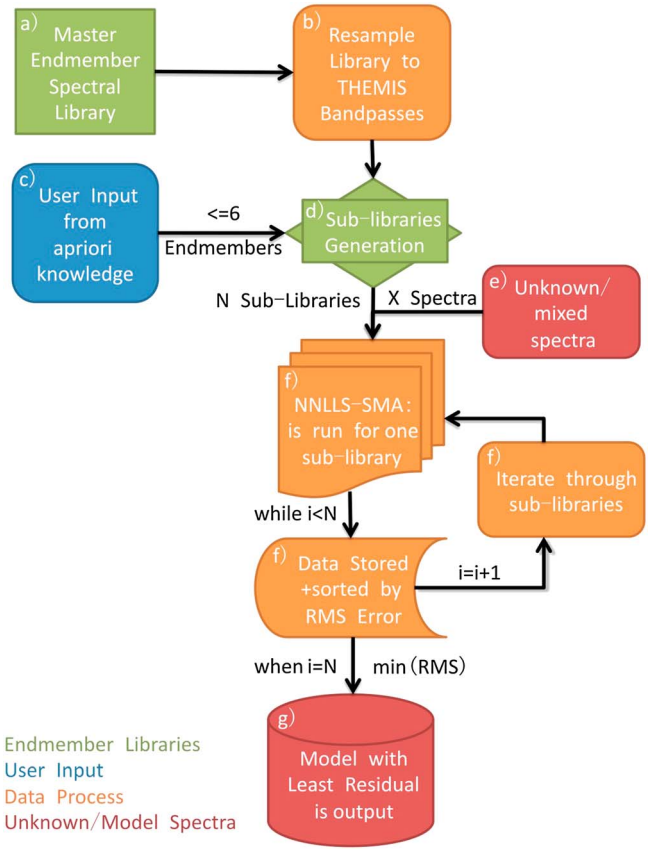


**Figure 1.** Flowchart of data and method used in this study. (a) Use mineral TIR spectra in Arizona State University (ASU) spectral library (http://speclib.asu.edu/) to build a master end-member spectral library. (b) Resample the spectra in the library to THEMIS band passes. (c, d) Select mineral groups based on apriori knowledge of the study region to generate sublibraries; the number of each sublibrary contains at most six minerals. (e) Extract unknown/mixed spectra from bands 3 to 9 of atmospheric-corrected THEMIS IR data. (f) Use every sublibrary to fit each mixed spectrum with nonnegative linear least square (NNLLS) [*Rogers and Aharonson*, 2008] algorithm and sort the fit results by RMS errors. (g) Output the fit result with least RMS error as the mineral determination result for each mixed spectrum.

component, plus a mineral of interest (e.g., olivine) to map the enrichment/depletion of the mineral of interest, related to the general basaltic component [e.g., *Rogers and Bandfield*, 2009]. However, understanding local- and regional-scale geologic processes requires quantitatively determined approximate abundances of major rock-forming minerals and not just a single mineral of interest.

[5] In this study, we developed least residual iterative spectral mixture analysis (LRISMA) to estimate major rock-forming mineral abundances with TIR multispectral data. Iterative spectral mixture analysis (SMA) approaches have been applied to both VNIR and TIR hyperspectral data [*Roberts et al.*, 1998; *Rogge et al.*, 2006; *Johnson et al.*, 2007], but LRISMA provides a new approach in the determination of quantitative mineralogy of small-scale geologic features (~1 $km^2$) on the surface of Mars with limited spectral resolution provided by current TIR imaging instruments.

## 2. Data

[6] In order to validate the LRISMA technique, we applied it to previously analyzed laboratory and TES spectra that were convolved to THEMIS band passes to simulate THEMIS spectra. These spectra and those from real atmospherically corrected THEMIS data used in this study are described below.

### 2.1. Laboratory Spectra

[7] To test the technique on well-characterized rocks, we selected a suite of laboratory-measured spectra, including 26 granitic rocks, 8 rhyolitic to andesitic rocks, and 9 andesitic to basaltic rocks [*Feely and Christensen*, 1999] whose mineral abundances were previously estimated from traditional petrographic methods with errors of ±5–15% [*Feely*, 1997]. All the spectra of the rock samples were obtained at 2 $cm^{-1}$ data spacing over ~1600–400 $cm^{-1}$ (6.25–25 μm) which includes the spectral range of THEMIS data (~6.78–14.88 μm). For detailed descriptions of all the samples, see *Feely* [1997]. The spectra were measured and calibrated using the method and instrument described by *Ruff et al.* [1997].

### 2.2. TES Spectra

[8] We used nine atmospherically corrected TES spectra averaged from global low-albedo regions [*Rogers and Christensen*, 2007]. These nine spectra are representative of

**Table 1.** Master Mineral Spectral Library[a]

| Mineral Group | End-Member | No. |
|---|---|---|
| Quartz | Quartz BUR-4120 | 1 |
| Feldspar | Microcline BUR-3460 | 2 |
| | Albite WAR-0244 | 3 |
| | Oligoclase WAR-5804 | 4 |
| | Andesine BUR-240 | 5 |
| | Labradorite WAR-4525 | 6 |
| | Bytownite WAR-1384 | 7 |
| | Anorthite BUR-340 | 8 |
| | Orthoclase WAR-RGSAN01 | 9 |
| Low-calcium pyroxene | Avg. Lindsley pigeonite | 10 |
| | Bronzite NMNH-93527 | 11 |
| | Enstatite HS-9.4B | 12 |
| | Hypersthene #NMNH-B18247 | 13 |
| High-calcium pyroxene | Augite NMHN-122302 | 14 |
| | Hedenbergite manganoan DSM-HED01 | 15 |
| | Diopside WAR-6474 | 16 |
| | Augite NMHN-9780 | 17 |
| Olivine | Forsterite BUR-3720A | 18 |
| | Fayalite WAR-RGFAY01 | 19 |
| | KI 3362 Fo60 | 20 |
| | KI 3115 Fo68 | 21 |
| | KI 3373 Fo35 | 22 |
| | KI 3008 Fo10 | 23 |
| High-silica | K-rich Glass | 24 |
| | opal-A (01–011) | 25 |
| Sheet silicate | Illite granular IMt-2 minus 60%bb[b] | 26 |
| | Ca-montmorillonite solid STx-1 | 27 |
| | saponite <0.2 mic plus 60%bb[b] | 28 |
| | Biotite BUR-840 | 29 |
| Amphibole | Magnesiohastingsite HS-115.4B | 30 |
| | Actinolite HS-116.4B | 31 |
| | Magnesiohornblende WAR-0354 | 32 |

[a]Mineral spectra are from the Arizona State University spectral library http://speclib.asu.edu [*Christensen et al.*, 2000a].
[b]Blackbody (uniform spectral emissivity = 1) was subtracted from the spectrum to produce comparable spectral contrast to solid samples.

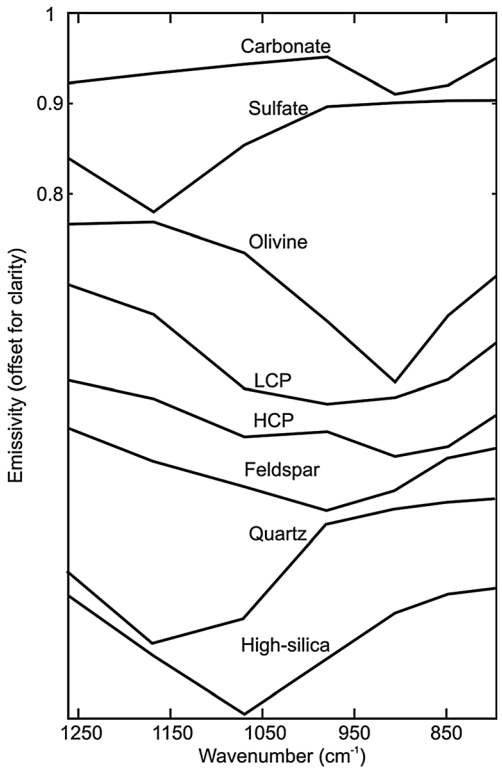


**Figure 2.** Simulated seven-band library spectra of different minerals. Spectra IDs in ASU spectral library are as follows: Quartz BUR-4120, Labradorite WAR-4524, Enstatite HS-9.4B, Augite NMNH-9780, KI 3115 Fo68, K-rich Glass, Anhydrite ML-S9, and Calcite C40.

the upper crust of Mars, and spectral analysis of them showed that Martian low-albedo regions are primarily composed of plagioclase, pyroxene, olivine, and high-silica phases. We also included the atmospherically corrected TES spectra of a quartz-rich crater central peak near Antoniadi crater described in *Bandfield et al*. [2004a] in order to apply LRISMA to spectra from more quartz-rich terrain.

### 2.3. THEMIS Data

[9] The THEMIS instrument onboard the Mars Odyssey spacecraft has been successfully operating for over 10 years. It acquires multispectral TIR images in 10 bands (6.78–14.88 μm; 100 m/pixel) and VNIR images in 5 bands (0.42–0.86 μm; 18–72 m/pixel) [*Christensen et al*., 2004]. The THEMIS instrument has two identical filters centered at 6.8 μm to increase the signal-to-noise ratio (SNR) in this wavelength band and designed to detect a specific carbonate feature [*Christensen et al*., 2004]. There are few locations on the surface where carbonate may be in high enough abundance to detect (e.g., Nili Fossae) [*Ehlmann et al*., 2008]. Since this region is not a target of interest of this work and because of the relatively low SNR of bands 1 and 2 [*Christensen et al*., 2004], we have elected to exclude these two bands to focus on major rock-forming minerals for the vast majority of Martian surfaces [e.g., *Rogers and Christensen*, 2007]. Furthermore, the band centered at 14.88 μm was designed to study atmospheric $CO_2$ [*Smith et al*., 2003] and it is also excluded from our analysis of the surface mineralogy. In order to test the method with real THEMIS TIR data, we selected an image (I01855008) with relatively warm temperatures (local solar time around 15:30) over the Mars Science Laboratory (MSL) landing site on the floor of Gale Crater and derived mineral abundances of low-albedo sand dunes. The mineralogy results we present may be verified by the MSL rover payload in the future.

## 3. Methods

[10] A detailed flowchart of the algorithm used in LRISMA is presented in Figure 1 and corresponds to tasks below, by subfigure numbers. Based on apriori knowledge from petrographic [*Feely*, 1997] and spectroscopic studies [*Bandfield*, 2002; *Murchie et al*., 2007; *Rogers and Christensen*, 2007], we generated a master spectral library of 32 laboratory spectra of minerals (Figure 1a and Table 1) for the spectral analysis. We excluded carbonate and sulfate minerals in this library mainly due to their absence in the rock samples [*Feely*, 1997] and low abundances in TES-derived

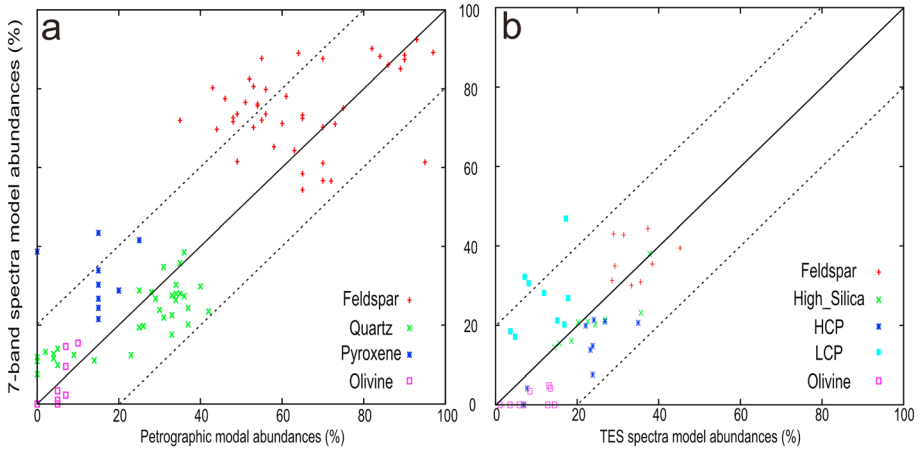


**Figure 3.** Mineral abundances determined by LRISMA and previous work. (a) Comparison of petrographic and simulated seven-band spectra modal analysis of igneous rock samples. The dashed lines represent ±20% of measured values and petrologic point count values. (b) Comparison of mineral abundances determined from TES spectra and simulated seven-band spectra analysis.

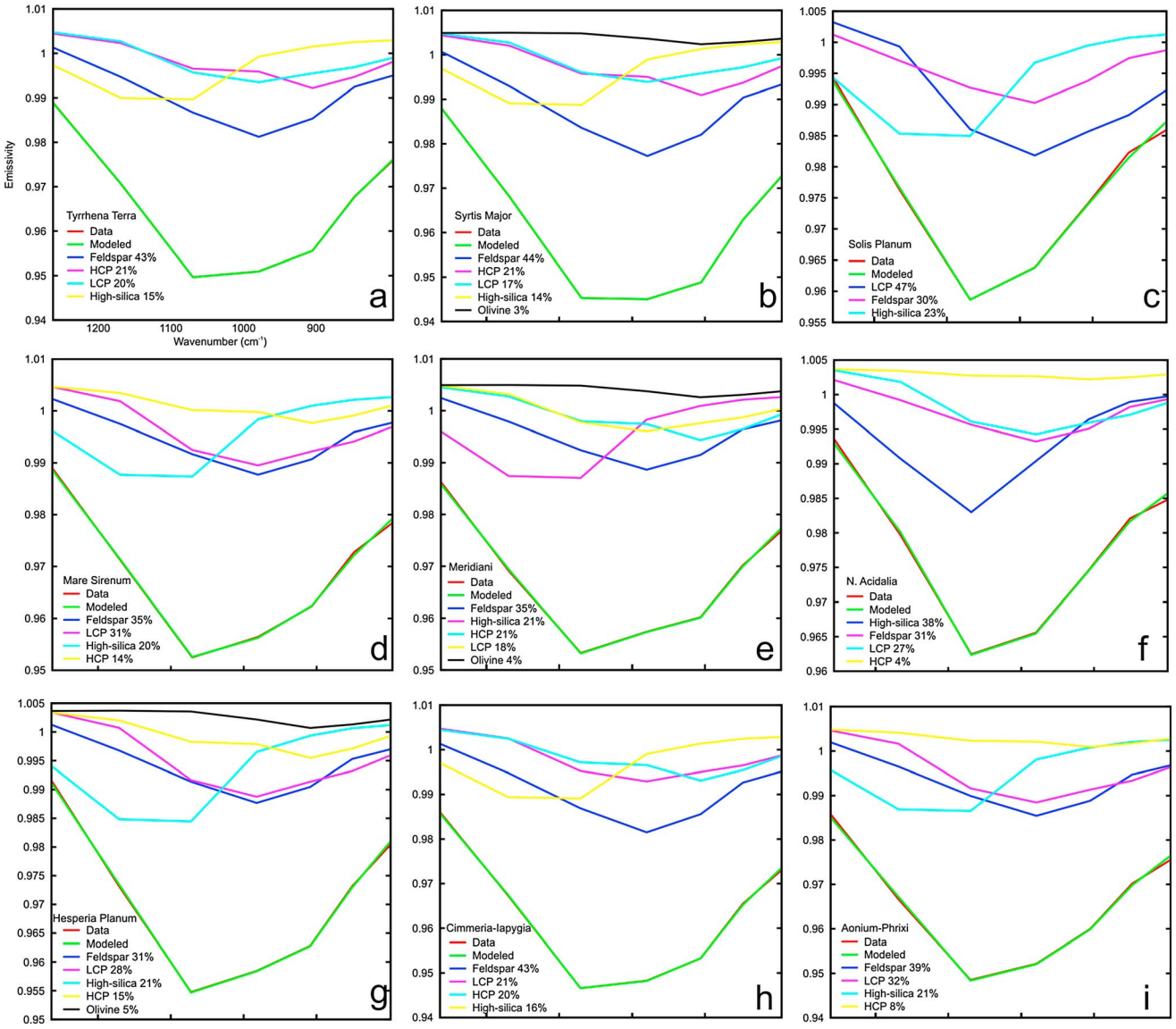


**Figure 4.** The seven-band spectra of each low-albedo region in *Rogers and Christensen* [2007] and the LRISMA model best fit including mineral end-members. Significant variations in spectral shapes remain after the TES spectra were convolved to THEMIS band passes.

surface compositions [*Rogers and Christensen*, 2007]. We then resampled the spectra using THEMIS IR imager spectral band-pass functions [*Christensen et al.*, 2004] and extracted seven-band spectra (centered at 7.93, 8.56, 9.35, 10.21, 11.04, 11.79, and 12.57 μm (1261, 1168, 1069, 979, 905, 848, and 795 $cm^{-1}$), Figure 1b). Examples of seven-band end-member spectra are shown in Figure 2. The target spectra mentioned in sections 2.1 and 2.2 were all resampled using the same methods as the library spectra to THEMIS seven-band spectra, while data in section 2.3 were simply extracted from an atmospherically corrected THEMIS observation (Figure 1e). Since both the target and the mineral end-member spectra are seven-band, six-mineral end-members (one band is preserved for blackbody) are at most allowed in the linear-unmixing (deconvolution) algorithm [*Ramsey and Christensen*, 1998].

[11] We then tailored sublibraries and mineral combinations from the master library for each group of target spectra as follows (Figures 1c and 1d):

[12] 1. For basaltic-andesite spectra in section 2.1, the sublibrary is composed of six olivines (Nos. 18–23), six feldspars (Nos. 3–8), and seven pyroxenes (Nos. 11–17). We generated 1890 unique sublibrary combinations by choosing one out of six olivines, two out of six feldspars, and two out of seven pyroxenes for every combination.

[13] 2. For granodiorite to rhyolite spectra in section 2.1, the sublibrary is composed of eight feldspars (Nos. 2–9), three amphiboles (Nos. 30–32), one quartz (No. 1), and one biotite (No. 29). 84 unique combinations were generated by selecting two out of eight feldspars, one out of three amphiboles, the quartz, and the biotite for every combination.

[14] 3. For atmospherically corrected TES spectra of global low-albedo regions described in section 2.2 and THEMIS spectra of dark sand dunes in Gale Crater described in section 2.3, we created a sublibrary composed of six olivines (Nos. 18–23), five feldspars (Nos. 4–8),

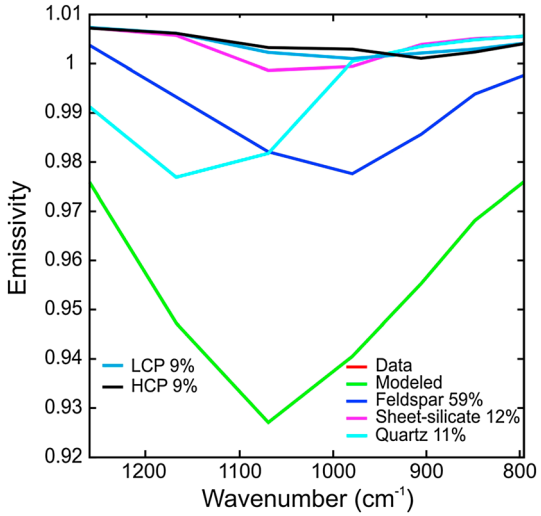


**Figure 5.** The simulated seven-band spectrum of quartzofeldspathic materials near Antoniadi Crater and the LRISMA model best fit.

two low-calcium pyroxenes (LCPs: Nos. 10 and 11), two high-calcium pyroxenes (HCPs: Nos. 14 and 15), and two high-silica phases (Nos. 24 and 25). 480 unique combinations were generated by selecting one out of six olivines, two out of five feldspars, one out of two LCPs, one out of two HCPs, and one out of two high-silica phases for every combination.

[15] 4. For the atmospherically corrected TES spectrum of quartzofeldspathic materials in section 2.2, the sublibrary is composed of eight feldspars (Nos. 2–9), seven pyroxenes (Nos. 10–12, 14–17), four high-silica phases and sheet silicates (Nos. 24, 26–28), and one quartz (No. 1). 1,176 unique combinations were generated by selecting two out of eight feldspars, one out of seven pyroxenes, two out of four high-silica phases or sheet silicates, and the quartz for every combination. More recent work has shown that quartz (TES/THEMIS) and hydrated silica (CRISM) are always found coincidentally [*Smith and Bandfield*, 2012]. However, we chose the spectra of this region to test the results of LRISMA when applying it to more quartz-rich terrain; therefore, we did not include hydrated silica in the sublibrary due to the exclusion of these spectra in the TES deconvolution of *Bandfield et al.* [2004a].

[16] The modified nonnegative [*Rogers and Aharonson*, 2008] linear least squares fitting technique [*Ramsey and Christensen*, 1998] was employed to model every seven-band target spectrum of the following (Figure 1f): (1) basaltic-andesite (1890 combinations); (2) granodiorite to rhyolite (84 combinations); (3) TES global low-albedo regions and the THEMIS spectrum of dark sand dunes in Gale crater (480 combinations); and (4) TES quartzofeldspathic materials (1176 combinations). Each model fit is characterized using the root-mean-square (RMS) error (a numeric characterization of the absolute difference between the model and the measured spectrum). The result of the least RMS for all the model fits was adopted as the best model mineralogy for each target spectrum (Figure 1g).

## 4. Results

### 4.1. Laboratory Igneous Samples

[17] The comparison of the mineral abundances determined by LRISMA and by petrographical studies [*Feely*, 1997] for library igneous samples is shown in Figure 3a. Data points that fall on the diagonal line represent perfect agreement between the two approaches for a particular phase. In general, mineral abundances derived from both methods agree in all samples: the one-sigma standard deviation of the difference (~66%) between results of LRISMA and the petrographical studies for feldspar, olivine, pyroxene, and quartz are ±16.1%, ±4.4%, ±10.4%, and ±8.5%, respectively. The overall reproducibility of LRISMA is ~5–20%, with model best fit results having values within these ranges. The reproducibility is calculated by the "sma" function of DaVinci software (http://

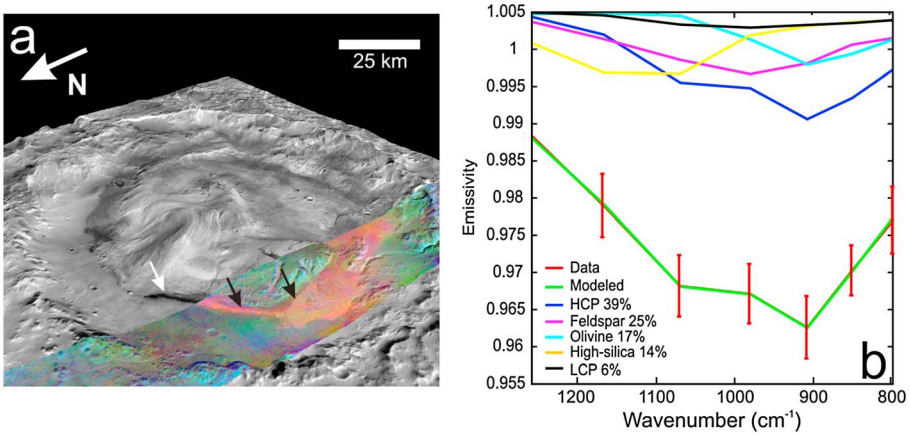


**Figure 6.** (a) THEMIS (I01855008) DCS (8-7-5 band) overlay on THEMIS-visible mosaic over Gale Crater. High Resolution Stereo Camera DTM (Digital Terrain Model) data (http://europlanet.dlr.de/node/fileadmin/pictures/hrsc/msl/dtm_msl_gc0911.da4.pds) are used for topography (5× vertical exaggeration). Dark sand dunes (white arrow) with elevated mafic composition are highlighted by orange color (black arrows). (b) Averaged seven-band spectra of 10 × 10 pixels (*x*: 75–84; *y*: 8425–8434) in Figure 6a and the LRISMA model best fit. The error bars show standard deviation of the average unknown spectrum.

davinci.asu.edu/index.php?title=sma), and the spectral fit result does not change within the range of reproducibility. The results shown in Figure 3a are in good agreement considering the significant degradation (seven bands) applied to the laboratory-measured spectra and the ~5–15% uncertainties in major minerals determined from petrographical studies [*Feely*, 1997]. Notably, the spectrally derived pyroxene abundances were overestimated, likely due to overlap of the longer wavelength features of pyroxene and olivine (see Figure 2).

### 4.2. TES Spectra

[18] *Rogers and Christensen* [2007] reported mineral abundances derived from the TES spectra presented in section 2.2. Significant variations in spectral shapes of the different low-albedo regions remain even after being convolved to THEMIS band passes. The seven-band spectra of each region and the best model fit including mineral end-members are shown in Figure 4. Good agreement exists between the mineral abundances derived from the simulated seven-band THEMIS spectra and the mineral abundances derived from TES deconvolution (Figure 3b). The one-sigma standard deviation of the difference between the feldspar, high-silica phases, HCP, LCP, and olivine abundances derived by the two models are ±7.3%, ±4.17%, ±4.96%, ±8.86%, and ±4.26%, respectively. The overall reproducibility of LRISMA is ~5–20%. However, olivine abundances were underestimated, while LCP abundances were overestimated, likely for the overlapping spectral features as stated above. For the spectrum of the quartzofeldspathic materials near Antoniadi Crater, LRISMA yielded $11 \pm 0.4\%$ quartz (Figure 5) compared to 7% quartz derived from TES data deconvolution reported in *Bandfield et al.* [2004a].

### 4.3. Application to THEMIS-Derived Surface Spectra

[19] We performed a running decorrelation stretch (DCS) [*Gillespie et al.*, 1986; *Edwards et al.*, 2011] on a THEMIS TIR image to highlight the surface compositional variations on the floor of Gale Crater (Figure 6a). The dark sand dunes are emphasized as an orange tone, indicating a relatively constant elevated mafic composition. Atmospheric components were removed to retrieve surface emissivity [*Bandfield et al.*, 2004b], and $10 \times 10$ spectra (~1 $km^2$) were averaged to increase the SNR (Figure 6b). All the derived mineral abundances are consistent with the results from TES data deconvolution (normalized from *Rogers and Bandfield* [2009]: feldspar 23.8%, pyroxene 35.7%, olivine 17.8%, and high-silica phases 22.6%).

## 5. Discussion

[20] Given the greatly reduced spectral resolution (seven bands) compared to laboratory (~600 bands) and TES (~73 bands after the removal of the atmospheric $CO_2$ region) spectral resolution, LRISMA resulted in a relatively accurate and reproducible determination of major rock-forming minerals for laboratory rock samples and for Martian surface materials with one-sigma errors of ~5–16% and ~4–9%, respectively. We have estimated that the overall reproducibility of LRISMA is ~5–20%.

[21] When examining the accuracy and reproducibility of LRISMA, three factors must be considered: (1) the errors in the "truth" data, where traditional petrographic mode estimates of rock thin sections have 5–15% errors for major minerals [*Feely*, 1997] and TES deconvolution results [*Christensen et al.*, 2001; *Rogers and Christensen*, 2007] have 5–15% errors depending on the mineral group. These errors would cause uncertainties along the $x$ axis for data points presented in Figures 3a and 3b; (2) the spectral range used for model fits (~1260–800 $cm^{-1}$) has been much reduced as compared to laboratory spectra (~1600–400 $cm^{-1}$) and TES spectra (~1300–200 $cm^{-1}$). Many diagnostic features of silicate minerals occur at lower wave numbers (<500 $cm^{-1}$), and the exclusion of this spectral region decreases the ability to definitively distinguish major rock-forming minerals. Limited bands and spectral range are expected to yield larger uncertainties as compared to TES spectral deconvolution results due to the lower number of controls of unique solutions of the linear system of equations; (3) although obvious spectral differences exist among different mineral groups (Figure 2), some major features overlap. For example, the main feature of olivine (~900 $cm^{-1}$) coincides with one of the main features of HCP and LCP at seven-band THEMIS spectral resolution (Figure 2). This overlapping spectral feature is likely the cause of the underestimation of olivine and overestimation of pyroxene mineral abundances.

[22] Multispectral unmixing has been successfully carried out in terrestrial remote-sensing studies [*Ramsey et al.*, 1999; *Scheidt et al.*, 2011], but the spectral shapes of mineral components in these studies are typically more distinct (e.g., quartz and carbonate-bearing rocks versus relatively small variations in nominally basaltic rocks) (Figure 2). For multispectral unmixing of Martian surface materials (mostly basaltic composition), preexisting knowledge about the mixed spectra is needed to generate sublibraries. The apriori component information could be derived from DCS of THEMIS images, VNIR (e.g., CRISM/ OMEGA), and regional TES spectral analysis.

## 6. Conclusions

[23] A new method has been applied to deconvolve seven-band THEMIS spectra to semiquantitatively determine the abundance of major rock-forming minerals including feldspar, pyroxene, olivine, high-silica phases, and quartz. Overall, the results agree well with petrographic studies and TES deconvolution results. This method provides a new way to refine the compositional abundances of small (~1 $km^2$) geologic features on planetary surfaces.

[24] **Acknowledgments.** The authors thank K. Murray and A. Deanne Rogers for providing spectral data used in this study. Discussions with M. Kraft, A. Ryan, and R. Smith are appreciated. JMARS and DaVinci team at Mars Space Flight Facility in ASU, especially D. Noss, aided in data processing. Christina Viviano, three anonymous reviewers, and Mark Wieczorek improved the quality of this paper. This project was supported by China Postdoctoral Science Foundation (2013M540614) and Postdoctoral International Exchange Project, Fundamental Research Founds for National University (CUG130106), and the Natural Science Foundation of China (41072045, 41373066).

## References

Bandfield, J. L. (2002), Global mineral distributions on Mars, *J. Geophys. Res.*, *107*(E6), 5042, doi:10.1029/2001JE001510.

Bandfield, J. L., V. E. Hamilton, P. R. Christensen, and H. Y. McSween (2004a), Identification of quartzofeldspathic materials on Mars, *J. Geophys. Res.*, *109*, E10009, doi:10.1029/2004JE002290.

Bandfield, J. L., D. Rogers, M. D. Smith, and P. R. Christensen (2004b), Atmospheric correction and surface spectral unit mapping using Thermal Emission Imaging System data, *J. Geophys. Res.*, *109*, E10010, doi:10.1029/2004JE002289.

Bell, J. (2008), *The Martian Surface: Composition, Mineralogy and Physical Properties*, Cambridge University Press, Cambridge, England.

Bibring, J. P., et al. (2006), Global mineralogical and aqueous mars history derived from OMEGA/Mars express data, *Science*, *312*(5772), 400–404, doi:10.1126/science.1122659.

Christensen, P. R., J. L. Bandfield, V. E. Hamilton, D. A. Howard, M. D. Lane, J. L. Piatek, S. W. Ruff, and W. L. Stefanov (2000a), A thermal emission spectral library of rock-forming minerals, *J. Geophys. Res.*, *105*(E4), 9735–9739, doi:10.1029/1998JE000624.

Christensen, P. R., J. L. Bandfield, M. D. Smith, V. E. Hamilton, and R. N. Clark (2000b), Identification of a basaltic component on the Martian surface from Thermal Emission Spectrometer data, *J. Geophys. Res.*, *105*(E4), 9609–9621, doi:10.1029/1999JE001127.

Christensen, P. R., et al. (2001), Mars Global Surveyor Thermal Emission Spectrometer experiment: Investigation description and surface science results, *J. Geophys. Res.*, *106*(E10), 23,823–23,871, doi:10.1029/2000JE001370.

Christensen, P. R., et al. (2004), The Thermal Emission Imaging System (THEMIS) for the Mars 2001 Odyssey Mission, *Space Sci. Rev.*, *110*(1–2), 85–130, doi:10.1023/B:SPAC.0000021008.16305.94.

Edwards, C. S., P. R. Christensen, and V. E. Hamilton (2008), Evidence for extensive olivine-rich basalt bedrock outcrops in Ganges and Eos chasmas, Mars, *J. Geophys. Res.*, *113*, E11003, doi:10.1029/2008JE003091.

Edwards, C. S., K. J. Nowicki, P. R. Christensen, J. Hill, N. Gorelick, and K. Murray (2011), Mosaicking of global planetary image datasets: 1. Techniques and data processing for Thermal Emission Imaging System (THEMIS) multi-spectral data, *J. Geophys. Res.*, *116*, E00G19, doi:10.1029/2010JE003755.

Ehlmann, B. L., et al. (2008), Orbital identification of carbonate-bearing rocks on Mars, *Science*, *322*(5909), 1828–1832, doi:10.1126/science.1164759.

Feely, K. C. (1997), *Quantitative Compositional Analysis of Igneous and Metamorphic Rocks Using Infrared Emission Spectroscopy*, Arizona State University, Tempe, Arizona.

Feely, K. C., and P. R. Christensen (1999), Quantitative compositional analysis using thermal emission spectroscopy: Application to igneous and metamorphic rocks, *J. Geophys. Res.*, *104*(E10), 24,195–24,210, doi:10.1029/1999JE001034.

Gillespie, A. R., A. B. Kahle, and R. E. Walker (1986), Color enhancement of highly correlated images. 1. Decorrelation and HSI contrast stretches, *Remote Sens. Environ.*, *20*(3), 209–235, doi:10.1016/0034-4257(86)90044-1.

Glotch, T. D., and P. R. Christensen (2005), Geologic and mineralogic mapping of Aram Chaos: Evidence for a water-rich history, *J. Geophys. Res.*, *110*, E09006, doi:10.1029/2004JE002389.

Hamilton, V. E., and P. R. Christensen (2005), Evidence for extensive, olivine-rich bedrock on Mars, *Geology*, *33*(6), 433–436.

Hamilton, V. E., P. R. Christensen, H. Y. McSween, and J. L. Bandfield (2003), Searching for the source regions of Martian meteorites using MGS TES: Integrating Martian meteorites into the global distribution of igneous materials on Mars, *Meteorit. Planet. Sci.*, *38*(6), 871–885, doi:10.1111/j.1945-5100.2003.tb00284.x.

Johnson, J. R., M. I. Staid, and M. D. Kraft (2007), Thermal infrared spectroscopy and modeling of experimentally shocked basalts, *Am. Mineral.*, *92*(7), 1148–1157, doi:10.2138/am.2007.2356.

Koeppen, W. C., and V. E. Hamilton (2008), Global distribution, composition, and abundance of olivine on the surface of Mars from thermal infrared data, *J. Geophys. Res.*, *113*, E05001, doi:10.1029/2007JE002984.

Mellon, M. T., B. M. Jakosky, H. H. Kieffer, and P. R. Christensen (2000), High-resolution thermal inertia mapping from the Mars Global Surveyor Thermal Emission Spectrometer, *Icarus*, *148*(2), 437–455, doi:10.1006/icar.2000.6503.

Murchie, S., et al. (2007), Compact Reconnaissance Imaging Spectrometer for Mars (CRISM) on Mars Reconnaissance Orbiter (MRO), *J. Geophys. Res.*, *112*, E05S03, doi:10.1029/2006JE002682.

Ramsey, M. S., and P. R. Christensen (1998), Mineral abundance determination: Quantitative deconvolution of thermal emission spectra, *J. Geophys. Res.*, *103*(B1), 577–596, doi:10.1029/97JB02784.

Ramsey, M. S., P. R. Christensen, N. Lancaster, and D. A. Howard (1999), Identification of sand sources and transport pathways at the Kelso Dunes, California, using thermal infrared remote sensing, *Geol. Soc. Am. Bull.*, *111*(5), 646–662, doi:10.1130/0016-7606.

Roberts, D. A., M. Gardner, R. Church, S. Ustin, G. Scheer, and R. O. Green (1998), Mapping chaparral in the Santa Monica Mountains using multiple endmember spectral mixture models, *Remote Sens. Environ.*, *65*(3), 267–279.

Rogers, A. D., and O. Aharonson (2008), Mineralogical composition of sands in Meridiani Planum determined from Mars Exploration Rover data and comparison to orbital measurements, *J. Geophys. Res.*, *113*, E06S14, doi:10.1029/2007JE002995.

Rogers, A. D., and J. L. Bandfield (2009), Mineralogical characterization of Mars Science Laboratory candidate landing sites from THEMIS and TES data, *Icarus*, *203*(2), 437–453, doi:10.1016/j.icarus.2009.04.020.

Rogers, A. D., and P. R. Christensen (2007), Surface mineralogy of Martian low-albedo regions from MGS-TES data: Implications for upper crustal evolution and surface alteration, *J. Geophys. Res.*, *112*, E01003, doi:10.1029/2006JE002727.

Rogers, A. D., and R. L. Fergason (2011), Regional-scale stratigraphy of surface units in Tyrrhena and Iapygia Terrae, Mars: Insights into highland crustal evolution and alteration history, *J. Geophys. Res.*, *116*, E08005, doi:10.1029/2010JE003772.

Rogers, A. D., P. R. Christensen, and J. L. Bandfield (2005), Compositional heterogeneity of the ancient Martian crust: Analysis of Ares Vallis bedrock with THEMIS and TES data, *J. Geophys. Res.*, *110*, E05010, doi:10.1029/2005JE002399.

Rogers, A. D., O. Aharonson, and J. L. Bandfield (2009), Geologic context of in situ rocky exposures in Mare Serpentis, Mars: Implications for crust and regolith evolution in the cratered highlands, *Icarus*, *200*(2), 446–462, doi:10.1016/j.icarus.2008.11.026.

Rogge, D. M., B. Rivard, J. Zhang, and J. Feng (2006), Iterative spectral unmixing for optimizing per-pixel endmember sets, *IEEE Trans. Geosci. Remote Sens.*, *44*(12), 3725–3736.

Ruff, S. W., P. R. Christensen, P. W. Barbera, and D. L. Anderson (1997), Quantitative thermal emission spectroscopy of minerals: A laboratory technique for measurement and calibration, *J. Geophys. Res.*, *102*(B7), 14,899–14,913, doi:10.1029/97JB00593.

Scheidt, S., N. Lancaster, and M. Ramsey (2011), Eolian dynamics and sediment mixing in the Gran Desierto, Mexico, determined from thermal infrared spectroscopy and remote-sensing data, *Geol. Soc. Am. Bull.*, *123*(7–8), 1628–1644, doi:10.1130/b30338.1.

Smith, M. R., and J. L. Bandfield (2012), Geology of quartz and hydrated silica-bearing deposits near Antoniadi Crater, Mars, *J. Geophys. Res.*, *117*, E06007, doi:10.1029/2011JE004038.

Smith, M. D., J. L. Bandfield, P. R. Christensen, and M. I. Richardson (2003), Thermal Emission Imaging System (THEMIS) infrared observations of atmospheric dust and water ice cloud optical depth, *J. Geophys. Res.*, *108*(E11), 5115, doi:10.1029/2003JE002115.

Tornabene, L. L., J. E. Moersch, H. Y. McSween Jr., V. E. Hamilton, J. L. Piatek, and P. R. Christensen (2008), Surface and crater-exposed lithologic units of the Isidis Basin as mapped by coanalysis of THEMIS- and TES-derived data products, *J. Geophys. Res.*, *113*, E10001, doi:10.1029/2007JE002988.